A Dramatic Odd–Even Oscillating Behavior for the Current Rectification and Negative Differential Resistance in Carbon-Chain-Modified Donor–Acceptor Molecular Devices

Zhenhua Zhang, Chao Guo, Denise Jeng Kwong, Jie Li, Xiaoqing Deng, and Zhiqiang Fan*

The donor–acceptor molecule is the only molecule that features a real intrinsic rectification. However, all investigations in the last decades showed that rectification behaviors of such molecules are not promising since their rectification ratio is only on the order of 10. Use of carbon chains C_n to serve as spacers is reported, along with attempts to modulate electrical behavior of the donor–acceptor molecule. Calculations using the first-principles method show that electrical behavior is indeed altered substantively, and a particular regularity can be clearly observed, i.e., a dramatic odd–even oscillation for electronic behavior with increasing carbon-chain length *n*. For models with even-*n* carbon chains, the rectification ratio is small (30), and no negative differential resistance (NDR) behavior is detected, but the rectifying performance of models with odd-*n* carbon chains is tremendously improved and rectification ratios on the order of 50 to 400 can be achieved, alongside a large NDR. This study thus suggests that using a suitable spacer might be an effective way to significantly boost electrical characteristics, including rectifying performance, of the donor–acceptor molecule.

1. Introduction

With the rapid development of microelectronics and the continuous miniaturization of conventional electronic devices, it is highly desirable to use a single molecule to construct an electronic device. Recent experimental and theoretical investigations show that molecular structures are capable of realizing basic electronic functions such as current rectification,[1–4] negative differential resistance (NDR),[5,6] electronic switching,[7,8] and transistor behavior,[9,10] etc. These results suggest that unimolecular electronics may play a key role in the design of future circuits. Particularly, the rectifying behavior and NDR phenomena of molecular devices have been investigated intensively due to their wide applications, such as in logic circuits, memory elements, amplification, and fast switching.

A diode called the D–σ–A molecular rectifier or A–R rectifier was first proposed by Aviram and Ratner[11] in 1974. Their purpose was to introduce the theoretical basis of rectifiers from a single molecule with a unique donor (D)–σ bridge (B)–acceptor (A) structure. This structure resembles the conventional semiconductor p–n junction and is considered to be the only molecular type that shows a real intrinsic rectifying behavior, which is completely different from other types of molecular rectification,[12] such as an asymmetric response of the molecular conformation to an interelectrode applied field, an asymmetric electrode material, or an asymmetric potential drop (either at molecule–electrode contacts or along the molecule) which leads to rectification. Therefore, donor–-acceptor molecular rectifiers have been studied widely. In 1997, Metzger et al.[13] experimentally discovered the first current rectification in Langmuir–Blodgett (LB) films of $C_{16}H_{33}Q$ – 3CNQ, which possesses well-defined donor and acceptor portions. However, Krzeminski et al.[14] attributed this observed rectification to an asymmetric profile of electrostatic potential across the system due to a geometrical asymmetry by the $C_{16}H_{33}$ tail, not to the A–R rectifying mechanism. In 2000, Ellenbogen et al.[15] introduced a package of donor–acceptor molecular models, but the calculations of Stokbro et al.[16] for these showed little or no rectifying behavior. Recently, Staykov et al.[17] presented that the obtained rectification ratio is only 7 for a donor–π–acceptor system. In our previous work,[18,19] we predicted theoretically that donor–acceptor molecules have a inverse rectification (maximum rectification ratio ≤ 14), namely, a larger (smaller) current occurs along the direction from the A(D) part to D (A) part, which disagrees completely with the prediction by Aviram and Ratner,[11] due to an always-existing asymmetric coupling of molecular orbitals to both electrodes.[18,19] Our theoretical finding has recently been confirmed experimentally by Yee et al.[20] So far, all investigations performed on simple donor–acceptor molecules seem not to be promising, as they have a rectification ratio only on the order of 10.[16–22] Accordingly, the issue of how to greatly enhance the rectification ratio of donor–acceptor molecules by novel ways and new mechanisms is an important one for studies of molecular rectifiers.

Prof. Z. Zhang, C. Guo, D. J. Kwong, J. Li,
Dr. X. Deng, Dr. Z. Fan
School of Physics and Electronic Science
Changsha University of Science and Technology
960S, Wanjiali Road, Sec. 2, Changsha 410114, China
Institute of Nanomaterial & Nanostructure
Changsha University of Science and Technology
960S, Wanjiali Road, Sec. 2, Changsha 410114, China
E-mail: lgzzhang@sohu.com

DOI: 10.1002/adfm.201201790

© 2013 WILEY-VCH Verlag GmbH & Co. KGaA, Weinheim

The NDR is a very important physical phenomenon typically observed in semiconductor devices in the resonant tunneling regime. In molecular electronics, the phenomenon and mechanism of NDR are currently attracting increasing exploratory efforts due to its promising potential applications, as stated above. NDR has been found in a variety of molecular devices, such as phenylethynylene oligomer (OPE) molecular junctions,[5,6] a single benzene ring with a nitro side group[23] or by an external gate field,[24] mirror-symmetrical straight carbon nanotube heterojunctions,[25] carbon nanowires contacted directly to two asymmetric electrodes,[26] a squashed C_{60} molecular device,[27] and a squeezed carbon monatomic ring,[28] etc. More recently, Prasongkit et al.[29] studied interference effects in phthalocyanine controlled by H–H tautomerization and found that gold–H_2Pc–gold junctions show pronounced NDR at high bias voltage, as well as weak NDR at intermediate bias. However, significant NDR has not yet been observed in a single donor–acceptor molecule.

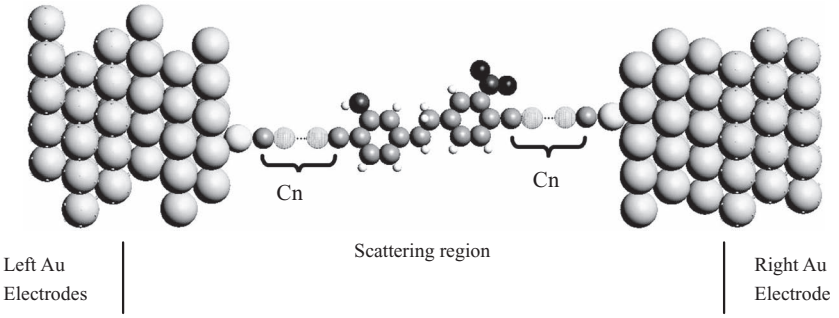

Figure 1. Structures of the molecular devices in our simulation. The phenylamine (left) and nitrobenzene (right) act as donor (D) and acceptor (A), respectively, and carbon chains C_n serve as the spacers between the D–σ–A molecule and Au electrodes, and number n is defined as the length of a carbon chain.

A carbon chain is an important chemical species, which has been extensively investigated both theoretically and experimentally.[30–40] Particularly, unimolecular devices consisting of carbon chains capped with pyridine groups at their two ends were recently assembled and measured using break-junction techniques.[35] All results hitherto showed that carbon chains have exceptional electronics characteristics.[29–40] For example, Lang and Avouris[37,38] reported that when carbon chains were connected directly to two Au electrodes, the zero-bias conductance would oscillate as a function of the number of carbon atoms in the chains. Recently, Prasongkit et al.[40] showed that the transmission spectrum and the conductance for carbon chains with a cumulene configuration depend only weakly on applied bias and the I–V characteristic is nearly linear over a bias region of ±1 V.

Herein, we use carbon chains C_n as spacers to modulate the electrical behavior of the donor–acceptor molecule. The purpose is to explore whether such a new configuration can induce high-performance rectification and a large NDR phenomenon. Interestingly, transport properties for carbon-chain-modified D–σ–A molecular devices are indeed enhanced substantively, and a particular regularity can be observed: the rectifying and negative differential resistance display a dramatic odd–even oscillating behavior with increasing carbon-chain length n. Models with odd-n carbon chains acting as spacers at both sides of the D–σ–A molecule have a significant rectifying performance with maximum rectification ratios in the order of 50 to 400 and remarkable NDR behavior, while for models with even-n carbon chains acting as spacers, the rectification ratio is smaller (30), and no NDR behavior is observed. These results mean that spacers of carbon chains with different length n could control and change transport properties of the D–σ–A molecule tremendously.

2. Device Model and Theoretical Method

Molecular devices consisting of the D–σ–A molecule coupled with two identical Au (111) electrodes through spacer-thiol groups in our simulation are illustrated schematically in **Figure 1**. The D–σ–A molecule in devices is designed as phenylamine (left) and nitrobenzene (right), connected via an insulating alkane (ethane), and carbon chains C_n serve as spacers at both sides of the molecule, where n is the number of carbon atoms in an atomic chain and is defined as the length of a carbon chain. By changing the length n (n = 2–9) of carbon atomic chains, we gain models M(C2), M(C3), M(C4), M(C5), M(C6), M(C7), M(C8), and M(C9), respectively. Each model is divided into three regions: left electrode, right electrode, and the scattering region. The scattering region involves the molecular core (D–σ–A molecule plus spacer-thiol group) and the first three gold layers on each side near it, which is in the self-consistent cycle to take into account the molecule–electrode coupling and the electrode screening effect. To construct such models, each molecular core is first optimized by a separate calculation based on density functional theory (DFT). Then, each core is introduced between two electrodes and initially chosen to sit upright on the electrode surfaces, where S atoms have a typical Au–S distance of 2.45 Å and an S atom on each side is positioned at the "hollow" site of Au atoms on the surfaces. Finally, the entire scattering region geometry is optimized until all residual forces on each atom are smaller than 0.05 eV $Å^{-1}$.

In our studies, geometric optimizations of the device region and first-principles transport calculations are performed by using DFT combined with the nonequilibrium Green's function (NEGF) method as implemented in the Atomistix ToolKit 11.2.3 (ATK11.2.3). We employ Troullier-Martins norm-conserving pseudopotentials to represent the atom core and linear combinations of local atomic orbitals to expand the valence states of electrons. The Perdew-Burke-Ernzerhof (PBE) formulation of the generalized gradient approximation (GGA) is used as the exchange-correlation functional. Single-zeta plus polarization (SZP) basis set for Au and H atoms and double-zeta plus polarization (DZP) basis set for other atoms are adopted. The current through a molecular junction as a function of the applied external bias can be calculated from the Landauer-like Equation 1,[41]

$$I = (2e/h)\int_{\mu_R}^{\mu_L} dE\, T(E, V)[f_L(E) - f_R(E)] \quad (1)$$

© 2013 WILEY-VCH Verlag GmbH & Co. KGaA, Weinheim

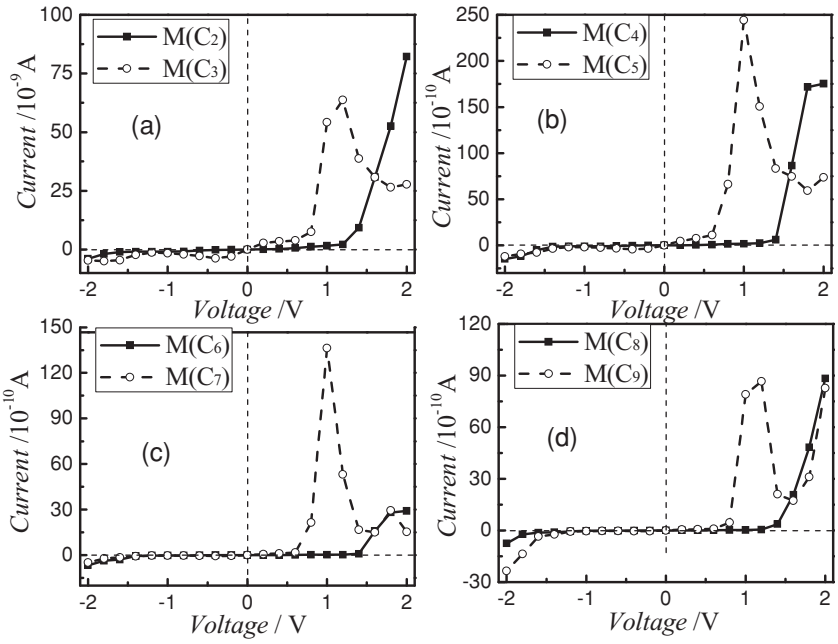

Figure 2. Current–voltage characteristics for all models. For M(C_{2i}) and M(C_{2i+1}) (where *i* is a positive integer), the models show obviously different nonlinear current–voltage characteristics.

3. Results and Discussions

3.1. Odd–Even Oscillating Behavior and Rectifying Analysis

Figure 2 shows our self-consistently calculated current–voltage (*I–V*) characteristics in the bias region from –2.0 to 2.0 V for all models. Evidently, transport properties are strongly dependent on the length *n* of spacer C_n and can be classified as two families by whether *n*'s value is even or odd, that is, models M(C_{2i}) and M(C_{2i+1}) (where *i* is a positive integer) show obviously different nonlinear current–voltage features. When models are positively biased, all M(C_{2i+1}) always open a significantly larger current earlier than all M(C_{2i}), and the especially noticeable NDR can be clearly observed in all M(C_{2i+1}) in the region of about 1.0 (or 1.2) to 1.8 V region, while no M(C_{2i}) shows any NDR. In contrast, the negative-bias current–voltage characteristics in all models are basically similar to each other, the electronic tunneling is extremely suppressed, and the currents always sustain a very small value. Therefore, highly asymmetric current–voltage characteristics for all models with respect to an inversion of bias are apparent.

Asymmetric current–voltage characteristics as stated above are generally evaluated by rectification ratio, the ratio of current values under positive and negative voltages for the same voltage magnitude, $R(V) = I(V)/|I(-V..)|$, as shown in **Figure 3**. Figure 3a presents the rectification ratio of all M(C_{2i}); the maximum values of the rectification ratio (RRmax) are 29.4 for M(C2) at

where μ_L (μ_R) is the chemical potential of the left (right) electrode, *V* is the electric potential difference between left and right electrodes, $V = (\mu_R - \mu_L)/e$, $\mu_R = E_f - V/2$, $\mu_L = E_f + V/2$, E_f is the Fermi level, set as zero, and thus $[-V/2, V/2]$ is a energy region contributing to the current integral and is called the bias window, and $f(E-\mu_L)$ and $f(E-\mu_R)$, respectively, are the Fermi distribution function of left and right electrodes. The transmission coefficient $T(E, V)$ as a function of the energy level *E* at a certain bias *V* can be calculated using the well-known Equation 2,

$$T(E, V) = Tr[\Gamma_L(E)G^R(E)\Gamma_R(E)G^A(E)] \quad (2)$$

where $G^R(E)$ and $G^A(E)$, respectively, are the advanced and retarded Green's functions of the scattering region, and $\Gamma'_{L(R)} = i\left(\sum^R_{L(R)} - \sum^A_{L(R)}\right)$ is the coupling functions of the conductor to the left and right electrodes, and $\sum^{R(A)}_{L(R)}$ is a self-energy matrix used to include effects of the left (right) semi-infinite electrode, which is explicitly included in the Kohn-Sham calculation for the extended molecular system. The value of this matrix can be determined by the Green's function technique using Equation 3,

$$\sum^{R(A)}_{L(R)} = C^+_{L(R)} G^{R(A)}_{L(R)} C_{L(R)} \quad (3)$$

where $C_{L(R)}$ is the coupling matrix of the molecule and the left (right) metallic electrode, and $G_{L(R)}$ is the Green's function of the semi-infinite electrode. All calculations are self-consistent under bias. The case in which the right (left) electrode is anode (cathode) is referred to as the application of a positive (or forward) bias.

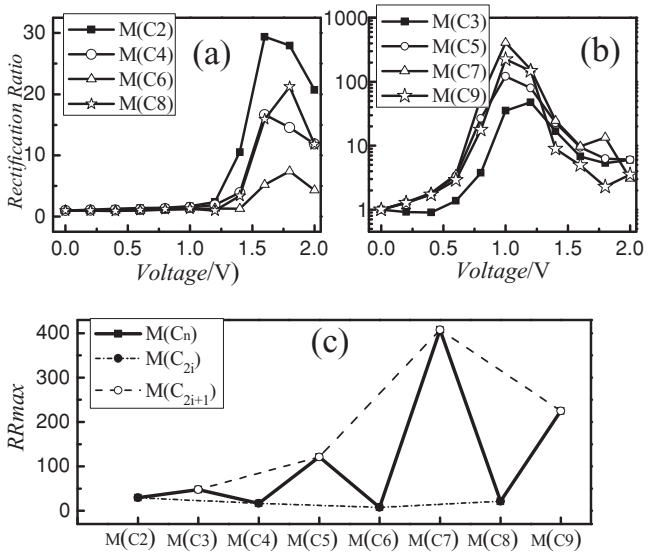

Figure 3. Variations of rectification ratios with bias for a) M(C_{2i}) and for b) M(C_{2i+1}). c) shows the change of maximum rectification ratios (RRmax) in all models with different lengths of spacers C_n, with a dramatic oscillation with increasing number of carbon atoms on chains.

© 2013 WILEY-VCH Verlag GmbH & Co. KGaA, Weinheim

Table 1. The spatial distribution of molecular states for all models at zero bias.

Molecular orbital	HOMO	LUMO
M (C2)	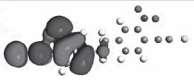	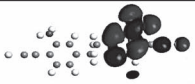
M(C3)	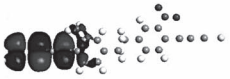	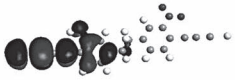
M(C4)		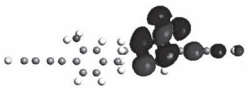
M(C5)		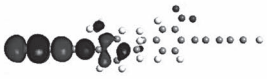
M(C6)	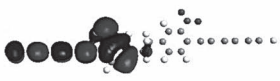	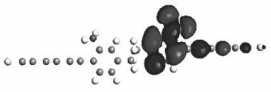
M(C7)		
M(C8)	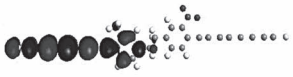	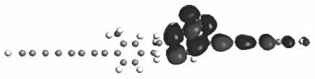
M(C9)		

1.6 V, 16.7 for M(C4) at 1.6 V, 7.43 for M(C6) at 1.8 V, and 22 for M(C8) at 1.8 V. Although these rectification ratios are not very large, they are enhanced to some extent over currently reported values for the D–A molecule, by an order of 10. Figure 3b shows the rectification ratio in all $M(C_{2i+1})$; the RRmax values are 48 for M(C3) at 1.2 V, 121 for M(C5) at 1.0 V, 408 for M(C7) at 1.0 V, and 225 for M(C9) at 1.0 V. Obviously, rectifying behaviors of the donor–acceptor molecule are predicted to be enhanced greatly by odd-*n* carbon chains acting as spacers.

The electronic tunneling and transport properties are intimately related to the spatial distribution of molecular eigenstates. We thus first plot the molecular projected self-consistent Hamiltonian (MPSH) eigenstates for all models to give a visual description of the electronic structure. The MPSH is the self-consistent Hamiltonian of the molecule in the presence of the Au electrode, and thus it contains the molecule–electrode coupling effects during the self-consistent iteration. **Table 1** displays the zero-bias spatial distribution of MPSH states for frontier orbitals; the lowest unoccupied molecular orbital (LUMO) and the highest occupied molecular orbital (HOMO). Interestingly, the states exhibit a distinctive regularity: for the LUMO state, the spatial distribution in models $M(C_{2i})$ and $M(C_{2i+1})$ is entirely different, that is, it is localized on the right side (nitrobenzene plus C_{2i}) for all $M(C_{2i})$ and on the left side (phenylamine plus C_{2i+1}) for all $M(C_{2i+1})$. However, for the HOMO state, its spatial distribution in models $M(C_{2i})$ and $M(C_{2i+1})$ is similar and always localized on the left side (phenylamine plus C_n). In other words, both frontier orbital states for $M(C_{2i})$ lie on the left side (phenylamine plus C_{2i}) and the right side (nitrobenzene plus C_{2i}). But frontier orbital states for $M(C_{2i+1})$ are all located on the left side (phenylamine plus C_{2i+1}). This observation means that frontier orbital states for $M(C_{2i+1})$ have a higher asymmetrically spatial distribution than that for $M(C_{2i})$. Moreover, by a careful inspection, one can also find that frontier orbitals of $M(C_{2i+1})$ are more localized than those of $M(C_{2i})$, since frontier orbitals of $M(C_{2i+1})$ are almost entirely limited to the left carbon chain C_{2i+1}, but frontier orbitals of $M(C_{2i})$ span over both carbon chain C_{2i} and benzene ring on the left side or the right side. In short, the spatial distribution of frontier orbitals in our models exhibits an evident even–odd behavior, which suggests a qualitative difference in the nature of electronic structure between the two types of models, $M(C_{2i})$ and $M(C_{2i+1})$. More importantly, all states are always localized (wholly or partially) on one of two carbon chains in a device rather than on two carbon chains simultaneously, which tends to increase asymmetries of local electronic structures along the electronic transport direction of our devices, and thus large rectification behaviors can be expected.

In Table 1, we can clearly see that the preferential structure of all carbon chains after the whole device is optimized is a polyyne configuration, with alternating single bonds of lengths of 1.33–1.35 Å and triple bonds with lengths of 1.20–1.23 Å. These bonding patterns can be explained easily. For the convenience of narration, carbon atoms on a chain are numbered 1C, 2C, 3C, …, and *n*C in the direction from the phenyl ring to S atom, where *n* is the total number of atoms on a pure carbon chain. As we know, in a phenyl ring, each carbon atom is connected to adjacent two carbon atoms by three bonds, therefore, when such a carbon atom is connected to atom 1C on a carbon chain end, the bond in between should be a single bond in a length of about 1.40 Å, in turn, a triple bond occurs between atoms 1C and 2C, a single bond is formed between atoms 2C and 3C, and so on. Note that when *n* is even, there is a triple bond between atoms (*n*–1) C and *n*C, and the C–S bonding length is about 1.60 Å, whereas if *n* is odd, there is a single bond between (*n*–1) C and *n*C atoms, and the C–S bonding length is about 1.55 Å. To check impacts of bonding patterns of carbon chains on electronic transport of our devices, we fix carbon chains as cumulenes for calculations and find that the *I*–*V* characteristics and rectification ratios only exhibit a small change as compared with carbon chains with polyyne bonding patterns.

More importantly, electronic transport for carbon chains strongly depends on the nature of the specific valence π states with twofold degeneracy.[37] Linear carbon chains, regardless of their bonding, all feature sp hybridization, that is, the 2s

© 2013 WILEY-VCH Verlag GmbH & Co. KGaA, Weinheim

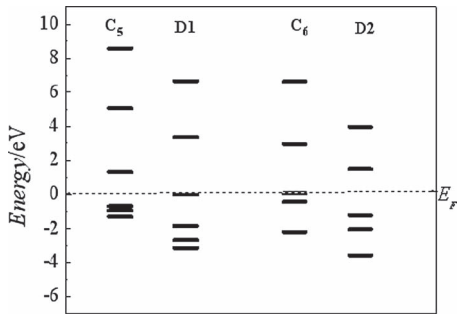

Figure 4. Energy levels in the proximity of Fermi level for carbon chains, C_5 and C_6, in an isolated situation, and for them in corresponding molecular devices, D1 and D2.

orbital is hybridized with the pz orbital to form two σ bonds, and the remaining p_x and p_y orbitals form a twofold-degenerate π orbital, i.e., $\varepsilon(p_x) = \varepsilon(p_y)$, where ε represents the orbital energy. Each carbon chain has two pairs of valence electrons which are not involved in bonding and are localized at the end carbon atoms. Thus, for a carbon chain with n atoms, $(n-1)/2$ degenerate π orbitals are fully occupied when n is odd, and $(n/2-1)$ degenerate π orbitals are fully occupied and the additional two electrons occupy the next higher orbital when n is even. This situation leads to the HOMO level being located below the Fermi level for odd-n chains and the Fermi level lying deeply in the HOMO level for even-n chains. When a carbon chain is connected onto Au electrodes, the situation is altered greatly. There is always a net transfer of electrons from electrodes to carbon chains due to their different electronegativities, which leads to the HOMO level just lying in the Fermi level for odd n chains and being located far below the Fermi level for even-n chains.[37] To demonstrate this issue more clearly, we take chains with carbon atoms $n = 5$ and 6 as examples. Energy levels in the proximity of Fermi level are displayed in **Figure 4**, where two carbon chains are denoted as C5 and C6, respectively. When the two chains are sandwiched between two Au electrodes to construct molecular devices, we define them as D1 and D2, respectively. Remarkably, the HOMO level just aligns with the Fermi level for $n = 5$ chain and locates far below the Fermi level for $n = 6$ chain in D1 and D2. Interestingly, from zero-bias HOMO levels respectively for groups $M(C_{2i+1})$ and $M(C_{2i})$ shown in **Figure 5**, one can clearly see this issue as well, which implies that carbon chains have a strong tuning ability on the electronic structure of the whole molecular compound.

When bias is applied, a system is driven out of equilibrium and molecular levels should shift for various complicated reasons, such as molecular successive polarizations (the spatial distribution of the charge density in the molecule is altered successively with the applied external electrical field (bias)), variations of the electrode potential, the potential drop profile in the whole device region, and the bias-dependent coupling strength between a molecule and electrodes with bias. As is well known, molecular orbitals provide possible transmission channels for electronic tunneling. Thus whether molecular orbitals enter into the bias window (BW) and their delocalization degree are underlying determinants of the transport properties, including rectifying performance. The evolution of molecular orbitals as a function of applied bias is shown in Figure 5. The Fermi level is set to zero. For simplicity, only molecular orbitals in the proximity of the Fermi level are displayed, which can move into or go close to the BW. As can be seen, two different groups are displayed for $M(C_{2i})$ and $M(C_{2i+1})$. For example, for M(C2) in group $M(C_{2i})$ under forward bias, LUMO and HOMO levels enter into the BW respectively around 1.4 and 1.2 V and contribute to a rapid increase of the current at such biases in Figure 2a, and the HOMO–LUMO gap (HLG) becomes narrower with an increase of bias. For a reversed bias, the HOMO level for $M(C_2)$ shifts away from the Fermi level at first, then toward the Fermi level about –0.4 V, and finally into the BW about –1.6 V, but the LUMO level always stays outside the BW. Therefore, the asymmetric shift of the LUMO and HOMO levels in M(C2) under biases of different polarities makes major and minor

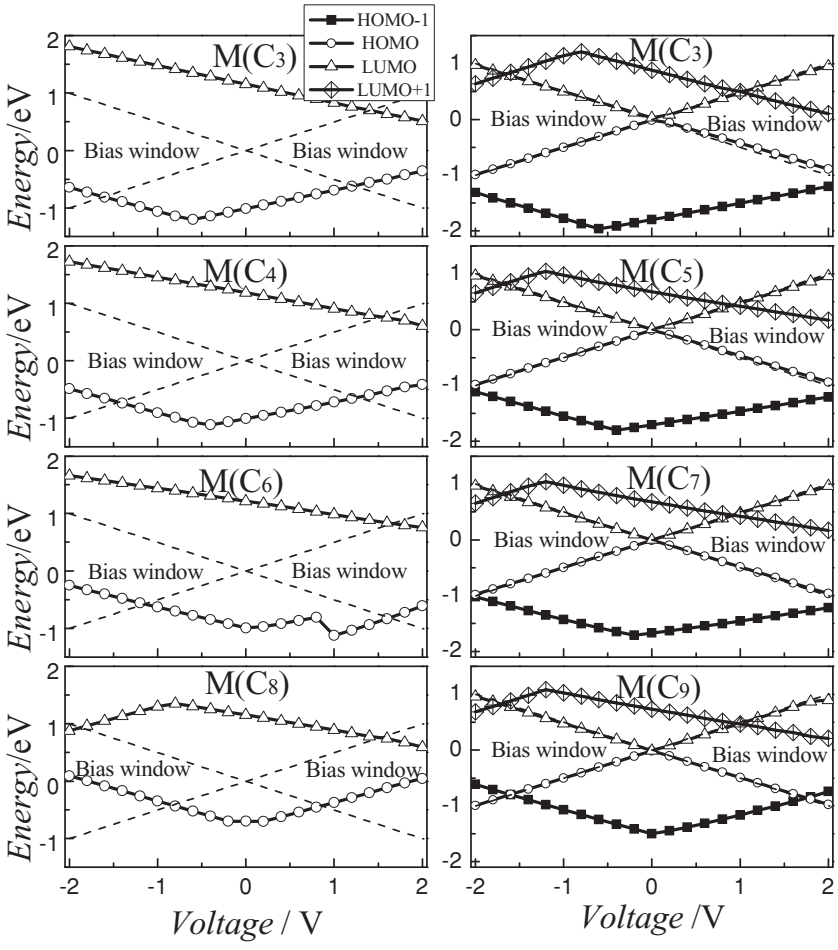

Figure 5. Evolution of the molecular orbitals under applied bias for all models.

© 2013 WILEY-VCH Verlag GmbH & Co. KGaA, Weinheim

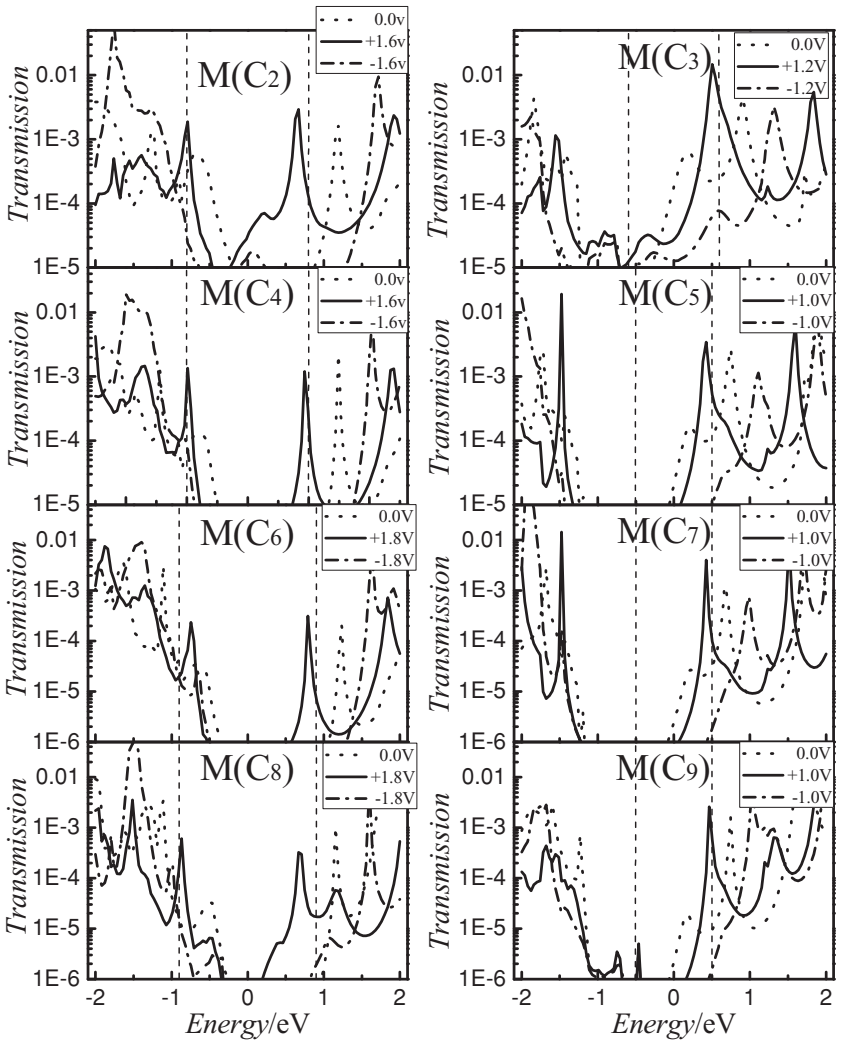

Figure 6. The transmission spectra of all models under three typical biases. The middle region of both dotted lines denotes the bias window.

contributions to a forward rectification, respectively. Features of other $M(C_{2i})$ are also qualitatively similar except for some distinctions of detail. Nevertheless, M(C3) in group $M(C_{2i+1})$ shows completely dissimilar characteristics to that in $M(C_{2i})$; HOMO and LUMO levels of this model almost always stick to the side of the BW under positive and negative biases except that the HOMO level somewhat moves into the BW under positive bias. Remarkably, the large rectification ratio of the M(C3) in group $M(C_{2i+1})$ essentially results from the LUMO+1 level which falls into the BW about +1.0 V and open a large current at a lower positive bias as compared with $M(C_{2i})$, whichthus leads to a larger forward rectification than for all $M(C_{2i})$. The situation for other $M(C_{2i+1})$ is basically identical. Interestingly, when a level enters into the BW at a high negative bias, we can see that a current rises but is not large, for example, for models in group $M(C_{2i+1})$. The reason for this issue is that the delocalization degree of LUMO states under high bias, including both high negative bias and high positive bias, is greatly weakened to decrease transmission resonance significantly, which was also found in a similar study by other authors.[16] This result can be related to the increasing field strength in the molecule which tends to increase the localization within the π-conjugated regions.[16] In fact, this point can also be observed clearly in the later Figure 8 and Figure 9.

In addition, we can observe different behaviors of the orbitals in their evolution with bias; this is because the spatial distribution of molecular states for different orbitals and their sensitivities to bias are different. The states localized at the sides are more sensitive to bias.[42] For example, the LUMO levels for group $M(C_{2i+1})$ can evolve with the V-type line. Our calculations show that these LUMO states are localized on the left carbon chains under positive bias but on the right carbon chains under negative bias since they are extremely sensitive to the direction of the external field (bias). This result implies that the LUMO states have a strong coupling with the left (right) electrode under positive (negative) bias so that these orbital levels always follow the left (right) electrode under bias.[20] As a result, the LUMO levels all shift toward the direction of positive energies under both positive and negative biases to form the V-type line.

As we know, the transmission spectra of devices are the most intuitive representation of quantum transport behaviors because the current through a device depends on the integral area of the transmission coefficient in the BW, according to a Landauer-like formula.[41] For clarity, **Figure 6** only shows the transmission spectra of all models at zero bias and several typical nonzero biases, which correspond to the best rectifying performance as shown in Figure 3. The incident electronic energies are set from −2.0 to 2.0 eV. Variations of transmission spectrum with bias are principally because a molecule can be polarized by the field, and this polarization is changeable, leading to bias-dependent transmission-spectrum curves. The position of transmission peak is generally determined by the energy level of the molecular orbital, i.e., transmission channel, and the delocalization degree of orbital directly affects the size of transmission peak. From Figure 6, one can see that for all $M(C_{2i})$, resonance peaks above and below the Fermi level arise from the LUMO and HOMO levels, which provides two major tunneling channels, and are involved inside the BW at +1.6 V (or +1.8 V). The transmission curve within the BW has a larger integrating area at a positive bias than that at a negative bias(−1.6 or −1.8 V), which is especially obvious for $M(C_2)$ and $M(C_8)$ and which leads to a forward rectification and a larger rectification for $M(C_2)$ and $M(C_8)$ compared to $M(C_4)$ and $M(C_6)$. For all $M(C_{2i+1})$, the resonance peak in the BW originates from LUMO+1, while highly localized LUMO and HOMO states that are almost entirely limited to the left carbon chain C_{2i+1}, as mentioned above, lead to a severe depression of the electronic tunneling, and no LUMO and HOMO transmission

© 2013 WILEY-VCH Verlag GmbH & Co. KGaA, Weinheim

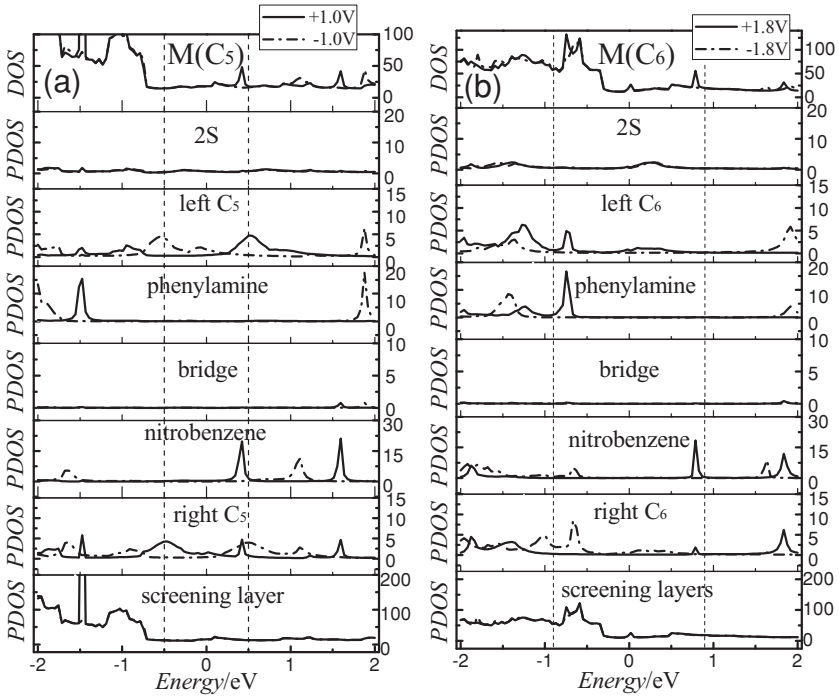

Figure 7. The device DOS and PDOS on several components of M(C5) and M(C6) at two typical biases. Vertical dash lines denote the bias window.

peaks are visible in Figure 6. The integrating area of the transmission curve within the BW is much larger at a positive bias (1.2 or 1.0 V) than at a negative bias (–1.2 or –1.0 V), especially obvious for M(C_7) and M(C_9). Meanwhile, we note that the magnitude of transmission peak(s) within the BW is much larger in all M(C_{2i+1}) than that in all M(C_{2i}). Thus we can expect that all M(C_{2i+1}) have a much larger forward rectification ratio than all M(C_{2i}), in particular, M(C_7) should possess the highest forward rectification ratio, and M(C_9) the next-highest.

To demonstrate the localized electronic structure in more detail and identify the contribution of various parts of a device to transport, especially for a rectifying performance; it is usually helpful to compute its projected density of states (PDOS) on an atom or a group of atoms, which can be obtained by summing the individual orbital PDOS contributions for an atom or a group of atoms. The orbital PDOS is the density of states projected on the ith atomic basis orbital $|\chi_i\rangle$, namely, PDOS = $\sum_{nk} \mathrm{Re}[c_i^*(E_{nk})\langle\chi_i \mid \psi(E_{nk})]\delta(E - E_{nk})$, where $|\psi(E)$ is a wave function for the device scattering state and could be presented as a linear combination of the pseudoatomic basis orbitals $|\chi_i\rangle$, $|\psi = \sum_i c_i |\chi_i\rangle$. E_{nk} are energies of incident states of electrons. Here we take models M(C5) and M(C6) as examples. The PDOS, as shown in **Figure 7**, is the density of states projected on six parts of the model: 2S, left C_n, phenylamine, σ-bridge, nitrobenzene, right C_n, and screening layers, at two typical biases, corresponding to maximum values of rectification ratios. The bias-polarity dependence of the DOS and PDOS can be clearly observed, which contributes to the rectification of a device. For the positively biased M(C_5), the positive-energy DOS peak in the BW, which can identified as the LUMO+1 peak just by looking at Figure 5, derives from the PDOS peaks of the nitrobenzene and the right C_5; this means that the LUMO+1 state lies on both nitrobenzene and on the right carbon chain, which is more delocalization than the HOMO and LUMO states have; these are only localized on the carbon chain, corresponding to the PDOS peak on the carbon chain in Figure 7a. Under negative bias, no DOS and PDOS peaks are found in the BW. As a result, a forward rectification for M(C_5) occurs. For M(C_6) under positive bias, two DOS peaks with positive and negative energies, corresponding respectively to the LUMO and HOMO states, emerge in the BW. Obviously, the LUMO state distributes on both nitrobenzene and the right C_6 chain, and the HOMO state on the phenylamine and left C_6. But under negative bias, only the negative-energy DOS peak that corresponds to the HOMO state contributed by the nitrobenzene and right C_6 (namely, the PDOS peaks of the right carbon chain and nitrobenzene line up to form the HOMO peak) can be inspected. Undoubtedly, there is a forward rectification for M(C_6). From the above detailed analysis, one can see a prominent carbon-chain effect, that is, the carbon chain is involved in almost all electronic tunneling channels, and thus the carbon chain plays a very important role in electronic transport for our devices. Furthermore, a negligibly small PDOS occurs on the σ-bridge; this implies that the σ-bridge is a well insulator that effectively prevents a mixture of states between acceptor and donor portions. It is worth noting that the PDOS analysis here on molecular states also rationalizes existing transmission peaks shown in Figure 6.

3.2. NDR Analysis

In the following, we will address the physical origin of the NDR behaviors observed in all M(C_{2i+1}), as demonstrated in Figure 2. For all M(C_{2i+1}), the LUMO+1 is responsible for the resonant tunneling at high positive bias, as shown in Figure 5. Therefore, the NDR behaviors for all M(C_{2i+1}) should be intimately related to this molecular orbital. **Figure 8** shows the transmission spectra for all M(C_{2i+1}) at two typical biases, which correspond to the peak and the valley of the current curve, as shown in Figure 2. From Figure 8 it is very clear that the LUMO+1 resonance is extremely sensitive to bias; this resonance shifts toward the Fermi level with increased bias and simultaneously reduces its resonance height greatly. As a result, the integrating area of the transmission coefficients within the bias window at a higher bias is much smaller than that at a lower bias, which leads to a large net drop of current and the NDR behavior occurs. In other words, the fact that the LUMO+1 resonance is greatly depressed with increased bias is the underlying physical origin of the NDR behavior observed in all M(C_{2i+1}).

To obtain the detailed information that molecular transmission channels are depressed on certain part(s) of a device with increased bias, we here select M(C_7) as an example to calculate

© 2013 WILEY-VCH Verlag GmbH & Co. KGaA, Weinheim

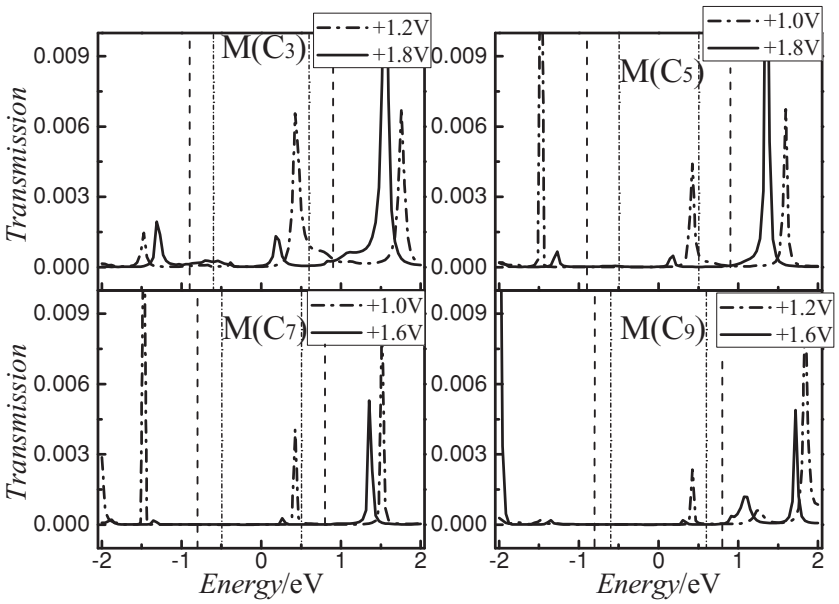

Figure 8. Bias-dependent transmission spectra for all $M(C_{2i+1})$ at biases that correspond to the peak and the valley of the current curve, as shown in Figure 2.

its PDOS at biases of 1.0 and 1.6 V, which correspond respectively to the peak and valley of the current curve. The projected parts are divided as shown in Figure 7. As can be seen from **Figure 9**, the LUMO+1 state is largely localized on the nitrobenzene and has only a small portion on the right C_7 chain. Strikingly, the height of the DOS peak of the LUMO+1 is reduced with increasing bias. By the PDOS, such a reduction can be unambiguously attributed to two factors. One factor is that the PDOS peak for the LUMO+1 on the nitrobenzene is suppressed with increasing bias; this is because increasing the field strength in the molecule tends to increase the localization of the molecular state within the π-conjugated region.[16] The other factor is a bias-driven energy mismatch of levels for different components of the molecular compound.[42,43] At 1.0 V, two PDOS peaks of the LUMO+1 for both nitrobenzene and right C_7 can be lined up strictly to form a high DOS peak. However, at 1.6 V, such a PDOS peak occurs at 0.32 eV for the nitrobenzene but at 0.21 eV for the right C_7, i.e., an energy mismatch occurs, which further reduces the DOS peak of the LUMO+1; that is to say, the bias-driven energy mismatch of levels between the nitrobenzene and the right C_7 and weakening of delocalization of the molecular state in the nitrobenzene are the origins of NDR here. Note that the DOS peak below the Fermi level mainly originates from the PDOS peak of screening layers (six layers of Au surfaces), which does not make any contribution to an effective electronic tunneling through a molecular core, thus it is unrelated to the rectification and NDR of a device.

Finally, we discuss the role played by thiol groups. As we know, thiol groups are introduced to act as "anchoring atoms" to form a stable structure for a molecular device, just like that in real experiments. Here, we are interested in the degree to which they affect the electronic transport. For this, we take $M(C_5)$ as an example and remove thiol groups at its both ends, and the remaining molecule compound is directly attached onto Au electrodes. Such a device is referred to as $M(C_5)^{RS}$. After it is fully relaxed, the *I–V* characteristic and rectification ratio are calculated and plotted in **Figure 10**. In comparation with calculated results for $M(C_5)$ as shown in Figure 2b and Figure 3b, we can clearly find that the shapes and trend of the *I–V* and rectification ratio curves for both $M(C_5)^{RS}$ and $M(C_5)$ are basically similar, including the NDR. Of course, there are also

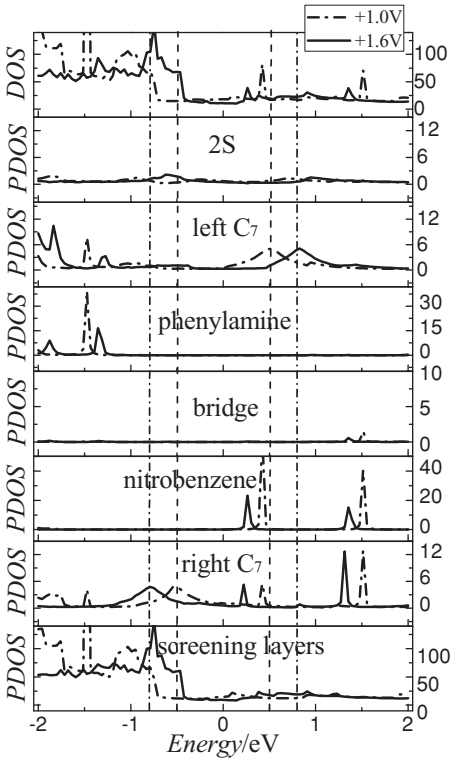

Figure 9. The device DOS and PDOS on several parts of $M(C_7)$ at two typical biases. Vertical dash lines denote the bias window.

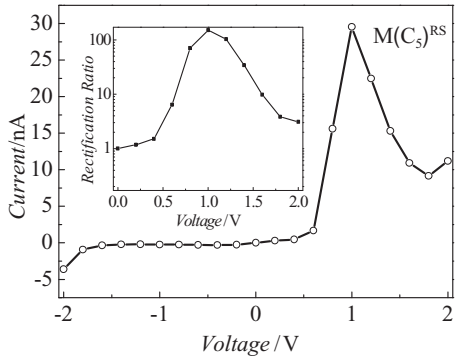

Figure 10. The *I–V* characteristics and rectification ratio (inset) for $M(C_5)^{RS}$. Clearly, they are similar to those for $M(C_5)$.

© 2013 WILEY-VCH Verlag GmbH & Co. KGaA, Weinheim

some detailed distinctions. For example, the maximum current is increased from 24.5 nA for $M(C_5)$ to 28.9 nA for $M(C_5)^{RS}$, and the maximum rectification ratio is enhanced from 121 for $M(C_5)$ to 131 for $M(C_5)^{RS}$. The variation of current can be attributed to changes of the molecular length and the energy-barrier size on the interface. Sulfur has a higher electronegativity than does carbon, therefore an S atom in a device would be more electron-dense, leading to the formation of a higher energy barrier to weaken electron tunneling. After S atoms at both ends of the molecule compound are removed, the energy barrier is reduced due to the lower electronegativity of C, and the molecular length becomes shorter as well, thus the current increases naturally. Here an enhanced rectification ratio more significantly highlights that effects of carbon chains on controlling rectification of the D–σ–A molecule are increased by removing S atoms. In other words, the interaction of carbon chains with the D–σ–A molecule, rather than S atoms, is responsible for the rectifying behaviors in our designed devices.

To examine the stability of our calculated results, we also calculated the electronic structures and transports with different exchange-correlation functions, such as local density approximation (LDA), or different basis sets, such as SZP for all atoms. We found that these variations result in only minor quantitative differences.

4. Conclusions

Motivated by recent investigations that show the donor–acceptor (D–A) molecule always possessing a very low rectifying performance (rectification ratio ca. 10), we explore how to enhance rectification ratio by novel ways and new mechanisms. We use carbon chains C_n with various lengths as spacers for the D–A molecule to construct molecular devices and a combination of density functional theory and nonequilibrium Green function formalism to study their electronic transport properties. A dramatic odd–even oscillation for transport behaviors with increasing carbon-chain length n can be clearly observed: for models with even-n carbon chains, the rectification ratio is smaller (30), and no negative differential resistance (NDR) behavior is detected. But for models with odd-n carbon chains, the rectifying performance is improved tremendously and maximum rectification ratios on the order of 50 to 400 can be achieved, which exceeds the limit of rectification ratio by 100 for a unimolecular rectifier using the currently accepted rectifying mechanism.[44] A large NDR behavior also appears. The new mechanism of high rectification ratio originates from the bias-polarity-dependent asymmetric shift of the LUMO+1 rather than the effects of frontier orbital (HOMO/LUMO) that were suggested by Aviram and Ratner. In short, asymmetric coupling of the molecule to electrodes is responsible for the rectification of our designed devices, that is, a level is pinned to the left (right) electrode chemical potential when its orbital is spatially located on the left (right) side of a device to cause an asymmetric movement of a molecular orbital under biases of different polarities. This effect is especially obvious for models with odd-n carbon chains acting as spacers, which have a correspondingly larger rectification ratio. These findings suggest that using a suitable spacer might be an effective way to significantly boost electrical characteristics, including rectifying performance, of the donor–acceptor molecule.

Acknowledgements

This work was supported by the National Natural Science Foundation of China (Grant Nos. 61071015, 61101009, and 61201080), the Construct Program of the Key Discipline in Hunan Province, Aid Program for Science and Technology Innovative Research Team in Higher Educational Instituions of Hunan Province, and the Innovation Foundation for Postgraduate in Changsha University of Science and Technology.

Received: July 1, 2012
Revised: November 14, 2012
Published online: January 11, 2013

[1] J. Taylor, H. Guo, J. Wang, *Phys. Rev. B* **2001**, *63*, 121104.
[2] I. I. Oleynik, M. A. Kozhushner, V. S. Posvyanskii, L. Yu, *Phys. Rev. Lett.* **2006**, *96*, 096803.
[3] J. B. Pan, Z. H. Zhang, K. H. Ding, X. Q. Deng, C. Guo, *Appl. Phys. Lett.* **2011**, *98*, 092102.
[4] H. Y. He, R. Pandey, G. Mallick, S. P. Karna, *J. Phys. Chem. C* **2009**, *113*, 1575.
[5] J. Chen, M. A. Reed, A. M. Rawlett, J. M. Tour, *Science* **1999**, *286*, 1550.
[6] M. Q. Long, K. Q. Chen, L. L. Wang, *Appl. Phys. Lett.* **2007**, *91*, 233512.
[7] S. J. van der Molen, J. H. Liao, T. Kudernac, J. S. Agustsson, L. Bernard, M. Calame, B. J. van Wees, B. L. Feringa, C. Schonenberger, *Nano Lett.* **2009**, *9*, 76.
[8] Z. C. Wang, T. Gu, T. Tada, S. Watanabe, *Appl. Phys. Lett.* **2008**, *93*, 152106.
[9] Y. Ren, K. Q. Chen, Q. Wan, B. S. Zou, Y. Zhang, *Appl. Phys. Lett.* **2009**, *94*, 183506.
[10] R. P. Andres, T. Bein, M. Dorogi, S. Feng, J. I. Henderson, C. P. Kubiak, W. Mahoney, R. G. Osifchin, R. Reifenberger, *Science* **1996**, *272*, 1323.
[11] A. Aviram, M. A. Ratner, *Chem. Phys. Lett.* **1974**, *29*, 277.
[12] R. Liu, S. Ke, W. Yang, H. U. Barange, *J. Chem. Phys.* **2006**, *124*, 024718.
[13] R. M. Metzger, B. Chen, U. Hopfner, M. V. Lakshmikantham, *J. Am. Chem. Soc.* **1997**, *119*, 10455.
[14] C. Krzeminski, C. Delerue, G. Allan, D. Vuillaume, *Phys. Rev. B* **2001**, *64*, 085405.
[15] J. C. Ellenbogen, J. C. Love, *Proc. IEEE* **2000**, *88*, 386.
[16] K. Stokbro, J. Taylor, *J. Am. Chem. Soc.* **2003**, *125*, 3674.
[17] A. Staykov, D. Nozaki, K. Yoshizawa, *J. Phys. Chem. C* **2007**, *111*, 11699.
[18] J. B. Pan, Z. H. Zhang, X. Q. Deng, M. Qiu, C. Guo, *Appl. Phys. Lett.* **2010**, *97*, 203104.
[19] J. B. Pan, Z. H. Zhang, X. Q. Deng, M. Qiu, C. Guo, *Appl. Phys. Lett.* **2010**, *98*, 013503.
[20] S. K. Yee, J. Sun, P. Darancet, T. D. Tilley, A. Majumdar, J. B. Neaton, R. A. Segalman, *ACS Nano* **2011**, *5*, 9256.
[21] R. Stadler, V. Geskin, J. Cornil, *J. Phys. Condens. Matter* **2008**, *20*, 374105.
[22] R. Stadler, V. Geskin, J. Cornil, *Adv. Funct. Mater.* **2008**, *18*, 1119.
[23] M. Di Ventra, S. G. Kim, S. T. Pantelides, N. D. Lang, *Phys. Rev. Lett.* **2001**, *86*, 288.
[24] M. Di Ventra, S. T. Pantelides, N. D. Lang, *Appl. Phys. Lett.* **2000**, *76*, 3448.
[25] X. F. Li, K. Q. Chen, L. L. Wang, M. Q. Long, B. S. Zou, *Appl. Phys. Lett.* **2007**, *91*, 133511.
[26] Q. Deng, J. C. Zhou, Z. H. Zhang, H. Zhang, M. Qiu, G. P. Tang, *Appl. Phys. Lett.* **2009**, *95*, 163109.

© 2013 WILEY-VCH Verlag GmbH & Co. KGaA, Weinheim

[27] Q. Fan, K. Q. Chen, Q. Wang, B. S. Zou, W. H. Duan, Z. Shuai, *Appl. Phys. Lett.* **2008**, *92*, 263304.
[28] M. Qiu, Z. H. Zhang, Z. Q. Fan, X. Q. Deng, J. B. Pan, *J. Phys Chem. C* **2011**, *115*, 11734.
[29] J. Prasongkit, A. Grigoriev, R. Ahuja, *Phys. Rev. B* **2011**, *84*, 165437.
[30] G. Roth, H. Fischer, *Organometallics* **1996**, *15*, 5766.
[31] C. H. Jin, H. P. Lan, L. M. Peng, K. Suenaga, S. Iijima, *Phys. Rev. Lett.* **2009**, *102*, 205501.
[32] K. H. Khoo, J. B Neaton, Y. W. Son, M. L. Cohen, S. G. Louie, *Nano Lett.* **2008**, *8*, 2900.
[33] Ž. Crljen, G. Baranović, *Phys. Rev. Lett.* **2007**, *98*, 116801.
[34] V. M. García–Suarez, C. J. Lambert, *Nanotechnology* **2008**, *19*, 455203.
[35] M. G. Zeng, L. Shen, Y. Q. Cai, Z. D. Sha, Y. P. Feng, *Appl. Phys. Lett.* **2010**, *96*, 042104.
[36] C. Wang, A. S. Batsanov, M. R. Bryce, S. Martin, R. J. Nichols, S. J. Higgins, V. M. García-Suarez, C. J. Lambert, *J. Am. Chem. Soc.* **2009**, *131*, 15647.
[37] N. D. Lang, Ph. Avouris, *Phys. Rev. Lett.* **1998**, *81*, 3515.
[38] N. D. Lang, Ph. Avouris, *Phys. Rev. Lett.* **2000**, *84*, 358.
[39] N. D. Lang, Ph. Avouris, *Phys. Rev. B* **2000**, *62*, 7325.
[40] J. Prasongkit, A. Grigoriev, G. Wendin, R. Ahuja, *Phys. Rev. B* **2010**, *81*, 115404.
[41] R. Landauer, *Philos. Mag.* **1970**, *21*, 863.
[42] D. Carrascal, V. M. García-Suarez, J. Ferrer, *Phys. Rev. B* **2012**, *85*, 195434.
[43] L. Chen, Z. Hu, A. Zhao, B. Wang, Y. Luo, J. Yang, J. G. Hou, *Phys. Rev. Lett.* **2007**, *99*, 146803.
[44] N. Armstrong, R. C. Hoft, A. McDonagh, M. B. Cortie, M. J. Ford, *Nano Lett.* **2007**, *7*, 3018.

© 2013 WILEY-VCH Verlag GmbH & Co. KGaA, Weinheim